Ultra-sensitive separation estimation of optical sources

Clémentine Rouvière, David Barral, Antonin Grateau, Ilya Karuseichyk,
Giacomo Sorelli, Mattia Walschaers, Nicolas Treps

HAL Id: hal-04430105

https://hal.sorbonne-universite.fr/hal-04430105v2

Submitted on 31 Jan 2024

OPTICA

Ultra-sensitive separation estimation of optical sources

Clémentine Rouvière,[1,*] **David Barral,**[1] **Antonin Grateau,**[1] **Ilya Karuseichyk,**[1] **Giacomo Sorelli,**[1,2] **Mattia Walschaers,**[1] **and Nicolas Treps**[1]

[1]*Laboratoire Kastler Brossel, Sorbonne Université, CNRS, ENS-Université PSL, Collège de France, 4 Place Jussieu, Paris, F-75252, France*
[2]*Fraunhofer IOSB, Ettlingen, Fraunhofer Institute of Optronics, System Technologies and Image Exploitation, Gutleuthausstr. 1, 76275 Ettlingen, Germany*
*clementine.rouviere@lkb.upmc.fr

Historically, the resolution of optical imaging systems was dictated by diffraction, and the Rayleigh criterion was long considered an unsurpassable limit. In superresolution microscopy, this limit is overcome by manipulating the emission properties of the object. However, in passive imaging, when sources are uncontrolled, reaching sub-Rayleigh resolution remains a challenge. Here, we implement a quantum-metrology-inspired approach for estimating the separation between two incoherent sources, achieving a sensitivity five orders of magnitude beyond the Rayleigh limit. Using a spatial mode demultiplexer, we examine scenes with bright and faint sources, through intensity measurements in the Hermite–Gauss basis. Analyzing sensitivity and accuracy over an extensive range of separations, we demonstrate the remarkable effectiveness of demultiplexing for sub-Rayleigh separation estimation. These results effectively render the Rayleigh limit obsolete for passive imaging. © 2024 Optica Publishing Group under the terms of the Optica Open Access Publishing Agreement

1. INTRODUCTION

The sensitivity and resolution of optical imaging systems play a crucial role in numerous fields ranging from microscopy to astronomy [1–5]. The core challenge, often used as a performance benchmark, is how precisely the separation between two incoherent point sources can be resolved. This key problem dates back to the late 19th century: the technological advances in microscopy and astronomy enabled scientists to observe objects at higher magnifications and with unprecedented levels of detail, but limited by diffraction. Understanding the fundamental principles that govern the behavior of light was essential to improve the resolution and accuracy of instruments. Thus, some of the leading optical physicists of the time turned their attention to this problem: Abbe [6], Rayleigh [7], and later Sparrow [8] proposed criteria based on visual benchmarks and diffraction properties of light. We know today that diffraction alone does not set a fundamental limit, but combined with detector characteristics and noise sources defines practical boundaries [9]. Super-resolution techniques that circumvent the diffraction limit have emerged over the last decades [10–14]. However, these domain-specific techniques are hitherto limited to certain types of microscopy. They require either intricate control over the light source [10,12] or manipulations of the illuminated sample [11,13]. Thus, these techniques are incompatible with passive imaging, where one does not control the properties of the light incoming from the scene to be imaged.

Passive imaging with spatially resolved intensity measurement, a strategy known as direct imaging (DI) that makes use of high-performance cameras, provides only a limited improvement and prevents substantial advancement beyond the limit imposed by the Rayleigh criterion [15]. However, recently, Tsang *et al.* [16] approached the historical problem of estimating the separation between two incoherent point sources by adopting the framework of quantum metrology. They demonstrated that the use of spatial-mode demultiplexing (SPADE) combined with intensity measurements is optimal, in the sense that it saturates the ultimate limit imposed by the laws of physics—the quantum Cramér–Rao bound [17–19]. SPADE provides a scaling advantage for the minimal resolvable distance compared with DI in an ideal scenario. This advantage is preserved in the presence of experimental noise even if the scaling is degraded [20–23]. The advantages provided by this metrology-inspired approach have been extended to optical imaging [24,25] and other related problems such as discrimination tasks [26,27] and multiparameter estimation [28–30], also including more general photon statistics [31,32], as well as entangled photon pairs [33], a context distinct from the setting under investigation in this study.

Early experiments used interferometric schemes to implement a simplified version of the demultiplexing approach [34–41], emulating the incoherence of the sources and restricting the estimation to short separations by accessing only two modes. Recently, multi-plane light conversion [42] has emerged as a promising technique for estimating separation, enabling a multimodal approach
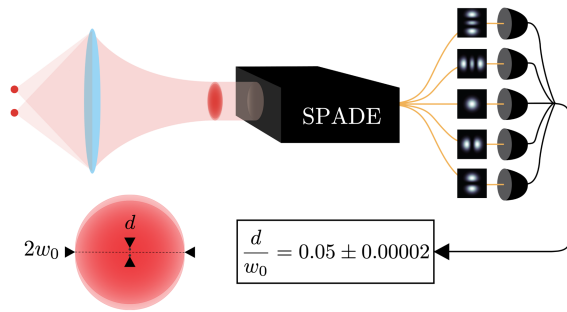
Fig. 1. Spatial-mode demultiplexing for separation estimation. SPADE consists of decomposing the incident light over the Hermite–Gaussian mode basis. Measuring the intensity corresponding to each mode was demonstrated to be an optimal measurement for transverse separation estimation. It gives a significant advantage with a gain of some orders of magnitude, compared to direct imaging, on the sensitivity of the estimation of close incoherent sources imaged through a diffraction-limited optical system. The numbers presented in this figure are typical results obtained with our experimental setup, where d is the transverse separation of two beams in the image plane, and w_0 is the waist of the beams in the same plane.

with the potential to reach the ultimate sensitivity at any separation. Two recent experiments explored this approach in different regimes: Boucher *et al.* [43] with equal-brightness sources and Santamaria *et al.* [44] with a strong brightness imbalance. They demonstrated that this technique is potentially efficient, but did not achieve an ultra-sensitive separation estimation.

Here, we implement separation estimation of two incoherent equally bright sources using spatial-mode demultiplexing over five spatial modes, combined with intensity measurements (see Fig. 1). For bright sources we directly measure a sensitivity up to five orders of magnitude beyond the Rayleigh criterion (in practice 20 nm sensitivity with 1 μm accuracy for a 1 mm beam size). For faint sources, we show performances unreachable with even ideal direct imaging (infinite resolution camera, no noise, equivalent losses) and demonstrate 20 μm precision for a 1 mm beam size and approximately 200 measured photons in the selected mode. Our experiment is the first practical demonstration of passive imaging going significantly beyond the Rayleigh limit, using a simple setup adaptable to standard passive imaging systems and with high-speed performance.

2. EXPERIMENTAL SETUP

The experimental setup is detailed in Fig. 2. The spatial-mode demultiplexing system is a multi-plane light converter (MPLC, Proteus-C from Cailabs). It decomposes an input light beam on the Hermite–Gaussian (HG) mode basis, each mode being subsequently coupled to a single-mode fiber. It allows for intensity measurements on several HG modes simultaneously. We use five MPLC outputs (out of 10) corresponding to the modes HG_{00}, HG_{01}, HG_{10}, HG_{02}, and HG_{20}. At the detection stage we use either photodiodes or single-photon avalanche-photodiodes depending on the input light flux.

Two incoherent optical sources are generated as follows: the light from a single fibered-telecom CW laser is split into two paths and goes through independent electro-optical modulators that apply random phases with high frequencies (see Supplement 1). The two incoherent guided modes are free-space coupled by collimators and combined on a beam splitter, thus mimicking the
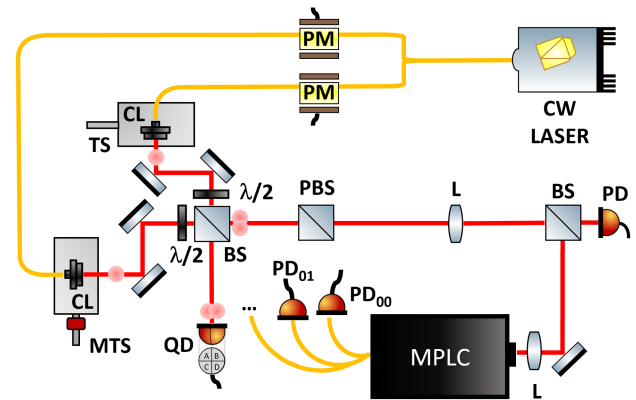

Fig. 2. Experimental setup. The two incoherent sources are generated from one continuous-wave fibered laser. The light is split into two paths that are modulated independently with two phase modulators (PM). The beams are then coupled into free space with collimators (CL) fixed either on a translation stage (TS) or on a motorized translation stage (MTS), which are used to set the separation between the two beams. The waist at the output of the collimators is 1.135 mm. The multiplexed beam is finally coupled into the multi-plane light converter (MPLC), whose intrinsic waist is around 320 μm, and the optical powers corresponding to HG modes (HG_{00}, HG_{01}, HG_{10}, HG_{02}, HG_{20}) are measured with photodetectors (PD_{00}, PD_{01} …). The reference separation is estimated by determining the position of each beam on a quadrant detector (QD), when the other source is turned off. An external photodiode (PD) is used for normalization in the high-flux regime.

images of two point sources separated by a set separation. They are mounted on independent translation stages so that the transverse separation between the two beams is adjustable. The two beams are Gaussian with similar sizes given by a waist of $w_0 \approx 1.135$ mm. The combined beam is imaged at the input of the MPLC, and mode-matched to its waist $w_1 \approx 320$ μm. A photodiode monitors the power stability, and half-wave plates combined with a polarizing beam splitter allow to balance the brightness of the two sources.

The measurement device is calibrated using only one source, with a position reference that is a quadrant detector in our case. Note that for single-source-position estimation the quadrant detector allows for close-to-Cramér–Rao-bound-limited estimation, and is thus a trustable reference [45]. The single beam is aligned and centered on the MPLC using the five HG modes intensities. Usage of all these modes, delivering information on both the centroid and mode-matching [46], is critical for the robustness and repeatability of the procedure. To proceed with calibration, the beam is translated in discrete steps whose position is determined with the quadrant detector (see Supplement 1), and the HG_{01}-mode output intensity is measured. This mode carries all the information necessary to estimate small transverse displacements ($\lesssim w_0$) [47], which is the regime we consider in this paper. Thanks to this precise procedure, this calibration can be done once and for all, and used for every estimation. It becomes a specification of the apparatus that does not need to be checked on a daily basis.

This calibration curve is used to perform parameter estimation. In our case, we make the hypothesis that the scene is composed of two identical incoherent sources and that the centroid is known. This information is used to compute a "two-source" calibration curve from the symmetrization of the apparatus calibration curve (see Supplement 1). It allows to infer the separation between two sources from the knowledge of the optical power in mode HG_{01}.

Then both optical sources are turned on; the beams are aligned and centered on the MPLC in an identical manner using the five HG output intensities and the quadrant detector. We perform a measurement as follows. First, the two beams are displaced symmetrically by a certain distance, keeping the centroid unchanged (the symmetry is guaranteed by the quadrant photodiode, but in this configuration, this photodiode is unable to deliver any information on the separation—see Supplement 1). Then the optical power at the output of the HG_{01} fiber is measured over a specific integration time. Finally, the separation is estimated using the "two-source" calibration curve. For each optical setting, this measurement is repeated 200 times in order to evaluate the statistical error of the measurement (the estimated separation is then the average of the 200 estimations, and the error on this value is given by the statistical standard deviation).

We estimated several separations in two intensity regimes (3500 and 10^{13} detected photons per integration time).

3. LOW-FLUX REGIME

We first present our results for the separation estimation between two faint sources, where the total incident power on the MPLC is around 50 fW during an integration time of 100 ms (resulting in 3500 detected photons). In Fig. 3, we plot the estimated separation as a function of the reference separation d_{ref}, for separations going from 400 μm up to 860 μm. We see a perfect linear trend and agreement between the measurement performed with the MPLC and the reference separation (obtained by measuring independently the position of each source with the quadrant detector—see Supplement 1).
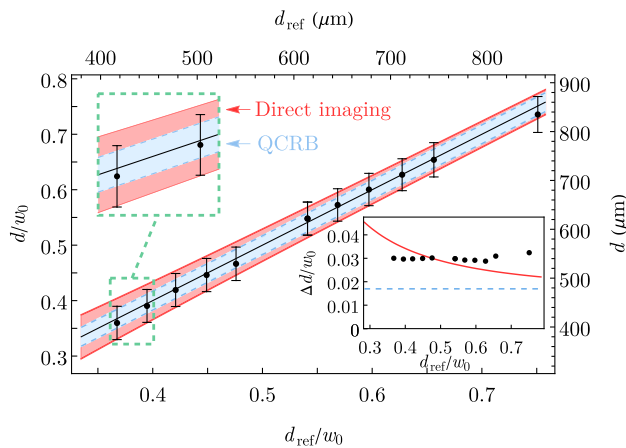

Fig. 3. Low-flux measurements. The separation estimation is realized with faint sources (3500 photons detected during 100 ms), using the mean value of the measured intensity corresponding to HG_{01} and the calibration curve. The estimated separations are plotted as a function of the reference separations determined with the quadrant detector. Both axes are presented with absolute values and values relative to the size of the beam. Error bars due to statistical uncertainty on the reference separation and the estimation, determined with 200 measurements (each during one integration time of 100 ms), are displayed as well as the unbiased estimation line (black line). The quantum Cramér–Rao bound—QCRB—(light blue) and the Cramér–Rao bound for ideal direct imaging (red) are also plotted as shaded areas for comparison. In the inset, we plot the sensitivity of the SPADE measurement as a function of the separation, along with the quantum Cramér–Rao bound (dashed blue line) and the Cramér–Rao bound for perfect direct imaging (red line), calculated for the same number of detected photons.

In order to benchmark the performance of the estimation we compute the statistical standard deviation, as explained in Section 2, and represent it as error bars on the experimental points in Fig. 3. We also plot this measurement sensitivity as a function of the separation in the inset of this figure. The measured sensitivity (around 33 μm) is very close to the quantum Cramér–Rao bound (19 μm when calculated for the same number of measured photons), the discrepancy arising from the level of dark counts of the detectors. As a matter of comparison, we also compute the classical Cramér–Rao bound for separation estimation with ideal direct imaging, considering infinitely small pixels, no noise, and the same detector quantum efficiency as for our experiment (see Supplement 1). Remarkably, our scheme outperforms this idealized DI setting for small separations (<500 μm). Furthermore, DI requires the measurement of all the photons (3500 in our case), increasing the influence of experimental noise, while modal decomposition allows to route the photons that carry information into a specific output of the MPLC (corresponding to the HG_{01} mode) and perform the detection on only 200 photons with a single detector to deliver an efficient estimator.

4. HIGH-FLUX REGIME

We consider now bright optical sources, which correspond to an incident power on the MPLC of around 650 μW for an integration time of 5 ms (or 10^{13} detected photons). Due to the scaling of the sensitivity versus the number of detected photons, we expect a much better sensitivity in this regime.

Similarly to the low-flux regime, we plot the estimated separation as a function of the reference separation in Fig. 4(a), for separations ranging from 20 μm to 160 μm. Once again, we note a perfect linear agreement between the measured separations and the reference ones. The reported error bars are computed from statistical error estimation. We can see in the inset of Fig. 4(a) that while these error bars are barely visible, the estimated separation deviates on average by approximately 1 μm from the reference separation. This deviation from unbiased estimation limits the accuracy of our system in the high-flux regime. This limitation can be traced back to the small differences between the two sources, because the two-source separation estimator is constructed from the single-source calibration under the hypothesis that both sources are identical. In practice the images of the sources have slightly different spatial shapes, which originates from how we generate them. This deviation amounts for the 1 μm limit (see Supplement 1). This is consistent with such an ultra-sensitive apparatus and is not due the detection system itself. In realistic scenarios, like microscopy or astronomy setups, this accuracy value will depend on the optical imaging device and the type of sources, and can eventually be largely improved.

To elucidate the full potential of our ultra-sensitive apparatus, we now focus on the statistical errors. To do so, we perform differential measurements: from a scene with a given separation between the two sources, for instance, 50 μm, only one source is displaced by a series of very small steps, of approximately 200 nm each. At each step, both separation and sensitivity estimations are performed. The results are displayed in the inset of Fig. 4(b), where we plotted the experimental points along with a linear fit as a guide for the eye. We observe in this case statistical errors of about 20 nm, and a linear trend consistent with the error bars. The slope of the linear fit is not equal to one, due to the limited accuracy; however, this demonstrates that our apparatus displays the unprecedented
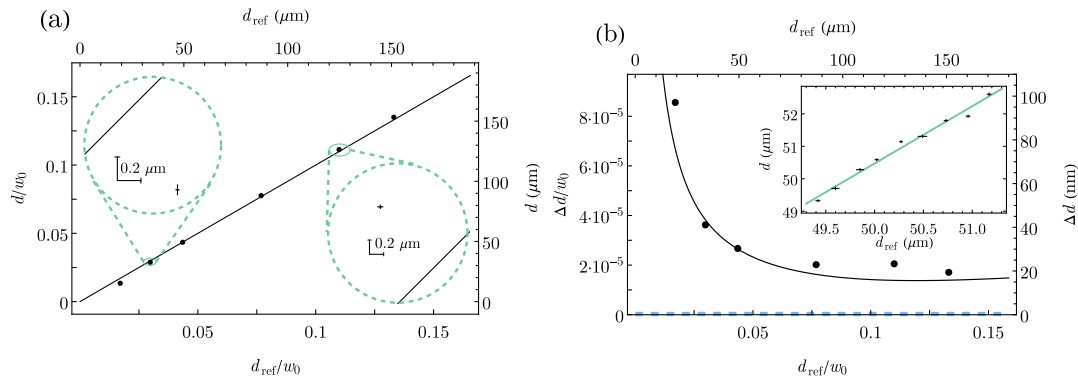
Fig. 4.   High-flux measurements. The separation estimation is realized with bright sources (10^{13} photons detected during 5 ms), using the mean value of the measured intensity corresponding to HG_{01} and the calibration curve. (a) The estimated separations are plotted as a function of the reference separations determined with the quadrant detector. Both axes are presented with absolute values and values relative to the size of the beam. Error bars due to statistical uncertainty on the reference separation and the estimation, determined with 200 measurements (each during one integration time of 5 ms), are displayed as well as the unbiased estimation line (black line). (b) The quantum Cramér–Rao bound (dashed blue line), which is 0.4 nm for 10^{13} detected photons, and the sensitivity for the SPADE measurement taking into account the detection noise (black line) are also plotted for comparison. In the inset, we plot the estimated separations versus the reference separations when performing a differential measurement. A separation of around 50 μm is fixed, and one source was displaced by several steps, each of approximately 200 nm. For each point, 200 measurements (each during one integration time of 5 ms) were realized to determine the statistical errors. The experimental points follow a linear tendency (green line).

ability to distinguish between two scenes with a difference in separation of the order of 20 nm. Note that some slight deviations from the estimated separation and the linear fit can be observed; this is to be expected in such an ultra-sensitive measurement where the actual scene is dependent on any mechanical or electronic noise (see Supplement 1).

Finally, we plot in Fig. 4(b) the sensitivity of source separation estimation versus the value of the separation and compare it to theoretical calculations. We demonstrate sensitivities ranging from 97 nm for our shortest separation of 20 μm to as low as 20 nm for larger separations. This corresponds to five orders of magnitude beyond the beam size. This feature is unique to our system, whose practicality is ensured by the single-source independent calibration (made possible by the information from multimode MPLC outputs). We compare these values to the quantum Cramér–Rao bound, which is 0.4 nm for 10^{13} detected photons. The difference is quantitatively reproduced by our theoretical model (see Supplement 1) taking into account the electronic noise of the detection apparatus, demonstrating that this is the limiting factor in our experiment. Note that this sensitivity corresponds to ≈ 5 nm at the input plane of the MPLC due to magnification 1/4 of the mode-matching telescope.

5. CONCLUSION

We realized a proof-of-principle experiment that demonstrates the practicability of modal decomposition for sub-diffraction separation estimation. We achieved a groundbreaking sensitivity in the estimation of the separation between two incoherent point sources for high and low brightness—beating the diffraction limit by five orders of magnitude and outperforming ideal direct imaging, respectively—thus setting a new standard in optical resolution. By leveraging the multimode nature of our experiment, we accomplished a robust calibration that led to this unprecedented level of sensitivity. Our system is simple to implement and can be adapted to advanced imaging systems, is fast and requires few detectors thus adaptable to any input light flux. Notably, reducing noise sources—particularly at the detection stage—could enhance the

separation-estimation sensitivity even further, eventually reaching the ultimate quantum limit.

Moreover, our singular scheme allows to explore more complex scenes. The source-phase modulation opens a new avenue for the study of tunable coherence situations [41]. In addition, an immediate extension of this work is the exploitation of the MPLC higher-order modes to estimate larger separations [48], but also for multi-parameter estimations [28,49], leading to a more complete scheme of passive imaging [24]. Finally, given the versatility of our approach and setup, we believe this framework can be further developed for applications in microscopy and astronomy within the near future.

Disclosures.   The authors declare no conflicts of interest.

Data availability.   Data underlying the results presented in this paper are not publicly available at this time but may be obtained from the authors upon reasonable request.

Supplemental document.   See Supplement 1 for supporting content.

REFERENCES

1. A. Labeyrie, S. G. Lipson, and P. Nisenson, *An Introduction to Optical Stellar Interferometry* (Cambridge University, 2006).
2. T. K. Henning, C. P. Dullemond, R. S. Klessen, and H. Beuther, *Protostars and Planets VI* (University of Arizona, 2014).
3. A. J. den Dekker and A. van den Bos, "Resolution: a survey," J. Opt. Soc. Am. A **14**, 547–557 (1997).
4. X. Nan, E. A. Collisson, S. Lewis, J. Huang, T. M. Tamgüney, J. T. Liphardt, F. McCormick, J. W. Gray, and S. Chu, "Single-molecule superresolution imaging allows quantitative analysis of RAF multimer

formation and signaling," Proc. Natl. Acad. Sci. USA **110**, 18519–18524 (2013).

5. D. Baddeley and J. Bewersdorf, "Biological insight from super-resolution microscopy: what we can learn from localization-based images," Annu. Rev. Biochem. **87**, 965–989 (2018).

6. E. Abbe, "Beiträge zur Theorie des Mikroskops und der mikroskopischen Wahrnehmung," Arch. Mikrosk. Anat. **9**, 413–468 (1873).

7. Rayleigh, "XXXI. Investigations in optics, with special reference to the spectroscope," London Edinburgh Dublin Philos. Mag. J. Sci. **8**(49), 261–274 (1879).

8. C. M. Sparrow, "On spectroscopic resolving power," Astrophys. J. **44**, 76 (1916).

9. N. Treps, N. Grosse, W. P. Bowen, C. Fabre, H.-A. Bachor, and P. K. Lam, "A quantum laser pointer," Science **301**, 940–943 (2003).

10. S. W. Hell and J. Wichmann, "Breaking the diffraction resolution limit by stimulated emission: stimulated-emission-depletion fluorescence microscopy," Opt. Lett. **19**, 780–782 (1994).

11. E. Betzig, G. H. Patterson, R. Sougrat, O. W. Lindwasser, S. Olenych, J. S. Bonifacino, M. W. Davidson, J. Lippincott-Schwartz, and H. F. Hess, "Imaging intracellular fluorescent proteins at nanometer resolution," Science **313**, 1642–1645 (2006).

12. S. W. Hell, "Far-field optical nanoscopy," Science **316**, 1153–1158 (2007).

13. R. M. Dickson, A. B. Cubitt, R. Y. Tsien, and W. E. Moerner, "On/off blinking and switching behaviour of single molecules of green fluorescent protein," Nature **388**, 355–358 (1997).

14. J.-E. Oh, Y.-W. Cho, G. Scarcelli, and Y.-H. Kim, "Sub-rayleigh imaging via speckle illumination," Opt. Lett. **38**, 682–684 (2013).

15. M. Shahram and P. Milanfar, "Statistical and information-theoretic analysis of resolution in imaging," IEEE Trans. Inf. Theory **52**, 3411–3437 (2006).

16. M. Tsang, R. Nair, and X.-M. Lu, "Quantum theory of superresolution for two incoherent optical point sources," Phys. Rev. X **6**, 031033 (2016).

17. C. Helstrom, "Resolution of point sources of light as analyzed by quantum detection theory," IEEE Trans. Inf. Theory **19**, 389–398 (1973).

18. V. Giovannetti, S. Lloyd, and L. Maccone, "Advances in quantum metrology," Nat. Photonics **5**, 222–229 (2011).

19. M. Barbieri, "Optical quantum metrology," PRX Quantum **3**, 010202 (2022).

20. M. Gessner, C. Fabre, and N. Treps, "Superresolution limits from measurement crosstalk," Phys. Rev. Lett. **125**, 100501 (2020).

21. Y. L. Len, C. Datta, M. Parniak, and K. Banaszek, "Resolution limits of spatial mode demultiplexing with noisy detection," Int. J. Quantum Inf. **18**, 1941015 (2020).

22. C. Lupo, "Subwavelength quantum imaging with noisy detectors," Phys. Rev. A **101**, 022323 (2020).

23. G. Sorelli, M. Gessner, M. Walschaers, and N. Treps, "Optimal observables and estimators for practical superresolution imaging," Phys. Rev. Lett. **127**, 123604 (2021).

24. A. Pushkina, G. Maltese, J. Costa-Filho, P. Patel, and A. Lvovsky, "Superresolution linear optical imaging in the far field," Phys. Rev. Lett. **127**, 253602 (2021).

25. K. K. M. Bearne, Y. Zhou, B. Braverman, J. Yang, S. A. Wadood, A. N. Jordan, A. N. Vamivakas, Z. Shi, and R. W. Boyd, "Confocal superresolution microscopy based on a spatial mode sorter," Opt. Express **29**, 11784–11792 (2021).

26. X.-M. Lu, H. Krovi, R. Nair, S. Guha, and J. H. Shapiro, "Quantum-optimal detection of one-versus-two incoherent optical sources with arbitrary separation," npj Quantum Inf. **4**, 1–8 (2018).

27. M. R. Grace and S. Guha, "Identifying objects at the quantum limit for superresolution imaging," Phys. Rev. Lett. **129**, 180502 (2022).

28. J. Řeháček, Z. Hradil, B. Stoklasa, M. Paúr, J. Grover, A. Krzic, and L. L. Sánchez-Soto, "Multiparameter quantum metrology of incoherent point sources: towards realistic superresolution," Phys. Rev. A **96**, 062107 (2017).

29. C. Napoli, S. Piano, R. Leach, G. Adesso, and T. Tufarelli, "Towards superresolution surface metrology: quantum estimation of angular and axial separations," Phys. Rev. Lett. **122**, 140505 (2019).

30. M. Tsang, "Subdiffraction incoherent optical imaging via spatial-mode demultiplexing," New J. Phys. **19**, 023054 (2017).

31. R. Nair and M. Tsang, "Far-field superresolution of thermal electromagnetic sources at the quantum limit," Phys. Rev. Lett. **117**, 190801 (2016).

32. C. Lupo and S. Pirandola, "Ultimate precision bound of quantum and subwavelength imaging," Phys. Rev. Lett. **117**, 190802 (2016).

33. F. Grenapin, D. Paneru, A. D'Errico, V. Grillo, G. Leuchs, and E. Karimi, "Super-resolution enhancement in bi-photon spatial mode demultiplexin," ArXiv, ArXiv:2212.10468 physics, [physics:quant-ph] (2022).

34. F. Yang, A. Tashchilina, E. S. Moiseev, C. Simon, and A. I. Lvovsky, "Far-field linear optical superresolution via heterodyne detection in a higher-order local oscillator mode," Optica **3**, 1148–1152 (2016).

35. M. Paúr, B. Stoklasa, Z. Hradil, L. L. Sánchez-Soto, and J. Rehacek, "Achieving the ultimate optical resolution," Optica **3**, 1144–1147 (2016).

36. Z. S. Tang, K. Durak, and A. Ling, "Fault-tolerant and finite-error localization for point emitters within the diffraction limit," Opt. Express **24**, 22004–22012 (2016).

37. W.-K. Tham, H. Ferretti, and A. M. Steinberg, "Beating Rayleigh's curse by imaging using phase information," Phys. Rev. Lett. **118**, 070801 (2017).

38. Y. Zhou, J. Yang, J. D. Hassett, S. M. H. Rafsanjani, M. Mirhosseini, A. N. Vamivakas, A. N. Jordan, Z. Shi, and R. W. Boyd, "Quantum-limited estimation of the axial separation of two incoherent point sources," Optica **6**, 534–541 (2019).

39. U. Zanforlin, C. Lupo, P. W. R. Connolly, P. Kok, G. S. Buller, and Z. Huang, "Optical quantum super-resolution imaging and hypothesis testing," Nat. Commun. **13**, 5373 (2022).

40. M. Parniak, S. Borówka, K. Boroszko, W. Wasilewski, K. Banaszek, and R. Demkowicz-Dobrzański, "Beating the Rayleigh limit using two-photon interference," Phys. Rev. Lett. **121**, 250503 (2018).

41. S. A. Wadood, K. Liang, Y. Zhou, J. Yang, M. A. Alonso, X.-F. Qian, T. Malhotra, S. M. H. Rafsanjani, A. N. Jordan, R. W. Boyd, and A. N. Vamivakas, "Experimental demonstration of superresolution of partially coherent light sources using parity sorting," Opt. Express **29**, 22034–22043 (2021).

42. J.-F. Morizur, L. Nicholls, P. Jian, S. Armstrong, N. Treps, B. Hage, M. Hsu, W. Bowen, J. Janousek, and H.-A. Bachor, "Programmable unitary spatial mode manipulation," J. Opt. Soc. Am. A **27**, 2524–2531 (2010).

43. P. Boucher, G. Labroille, C. Fabre, and N. Treps, "Spatial optical mode demultiplexing as a practical tool for optimal transverse distance estimation," Optica **7**, 1621–1626 (2020).

44. L. Santamaria, D. Pallotti, M. S. de Cumis, D. Dequal, and C. Lupo, "Spatial-mode-demultiplexing for enhanced intensity and distance measurement," arXiv, arXiv:2206.05246 (2023).

45. C. Fabre, J. B. Fouet, and A. Maître, "Quantum limits in the measurement of very small displacements in optical images," Opt. Lett. **25**, 76–78 (2000).

46. V. Chille, P. Banzer, A. Aiello, G. Leuchs, C. Marquardt, N. Treps, and C. Fabre, "Quantum uncertainty in the beam width of spatial optical modes," Opt. Express **23**, 32777–32787 (2015).

47. V. Delaubert, N. Treps, M. Lassen, C. C. Harb, C. Fabre, P. K. Lam, and H.-A. Bachor, "TEM 10 homodyne detection as an optimal small-displacement and tilt-measurement scheme," Phys. Rev. A **74**, 053823 (2006).

48. G. Sorelli, M. Gessner, M. Walschaers, and N. Treps, "Moment-based superresolution: formalism and applications," Phys. Rev. A **104**, 033515 (2021).

49. J. Řeháček, M. Paúr, B. Stoklasa, Z. Hradil, and L. L. Sánchez-Soto, "Optimal measurements for resolution beyond the Rayleigh limit," Opt. Lett. **42**, 231–234 (2017).